
Article:
Shi, Z., Zhong, Hai, Fan, W. J. et al. (2 more authors) (2019) Nanoscale probing of asymmetric magnetization reversal in perpendicularly exchange biased Pt/Co/Pt/IrMn multilayers. Journal of Magnetism and Magnetic Materials. pp. 127-131. ISSN 0304-8853

https://doi.org/10.1016/j.jmmm.2018.10.128

Nanoscale Probing of Asymmetric Magnetization Reversal in Perpendicularly Exchange Biased Pt/Co/Pt/IrMn Multilayers

Z. Shi[1*], H. Zhong[2,3†], W. J. Fan[1], S. M. Zhou[1], J. Yuan[2,4]

[1]*Shanghai Key Laboratory of Special Artificial Microstructure Materials and Technology & School of Physics Science and Engineering, Tongji University, Shanghai 200092, People's Republic of China,*

[2]*Beijing National Center for Electron Microscopy, Tsinghua University, Beijing 100084, People's Republic of China,*

[3]*Institute of Applied Physics, University of Hamburg, Jungiusstrasse 9a, 20355 Hamburg, Germany.*

[4]*Department of Physics, University of York, Heslington, York YO10 5DD, UK*

(Dated: October 20, 2018)

*Email: shizhong@tongji.edu.cn

†Email: hzhong@physnet.uni-hamburg.de

Abstract

Asymmetric magnetization reversal in perpendicularly exchange biased Pt/Co/Pt/IrMn multilayers was studied in nanometer scale by non-contact magnetic force microscopy with variable highly localized bipolar magnetic fields of the MFM tip. The hysteresis process of domain nucleation and pinned domain wall motion has been triggered and mapped simultaneously through MFM. Unstable magnetization reversal of submicron domains has been directly observed as well as exchange bias induced asymmetry in the depinning fields for domain wall motion. The current results demonstrated a possible way to locally *mapping* and *manipulating* novel magnetic nano-structures such as vortices and Skyrmions.

PACS numbers: 71.70.Et; 68.37.Rt; 75.60.Jk

I. INTRODUCTION

Exchange bias (EB) in coupled ferromagnet (FM) and antiferromagnet (AF), discovered by Meiklejohn and Bean in 1956[1], has been widely studied in the light of both fundamental mechanisms in physics and abundant technologies in modern spintronics[2,3]. The EB effect manifests itself by a horizontal shift (H_E) and an enhanced coercivity (H_C) of the hysteresis loop due to interfacial coupling between surface FM spins and uncompensated AF spins, which are either non-rotatable or rotatable[4]. All these AF spins are randomly distributed and highly localized[4–6]. Recently, EB has attracted renewed attention for its central role as the pinning/biased layer in the spin-valve devices[7]. In order to meet the industrial demand of high density non-volatile memory such as magnetic random access memory (MRAM), the size of magnetic domains is continuously reduced and the nano-dimensional effect of EB is intensively investigated[7–16]. Furthermore, room temperature vortices and Skyrmions have been demonstrated in antiferromagnet based heterostructure due to the strong Dzyaloshinskii-Moriya interaction (DMI) in AF/FM bilayers such as IrMn/CoFeB.[17,18] On the other hand, manipulating and controlling magnetic nanostructures are the key issues towards the utilization of new magnetic nanostructures. Owing to the spin-transfer torque and spin-orbit torque effect, the nanostructures such as vortices and Skyrmions can be created and moved by short-pulse, high density current[19,20]. By employing the MOKE microscopy, spin polarized low-energy electron microscopy (SPLEEM), XMCD-PEEM, Lorentz transmission electron microscopy and topological Hall effect, the special formations of magnetic nanostructure can be determined[19–26]. Due to its high spatial resolution, direct imaging and low cost, the magnetic force microscopy (MFM), working as a conventional high resolution magnetic mapping method, shows its advantage in probing the magnetic nanostructures[24–26]. MFM has been utilized to study the domain reversal in patterned films with in-plane exchange bias [27,28], as well as exchange biased vortices in submicron disk [29]. Asymmetric domain reversal has been studied in perpendicular exchange biased $[Co/Pt]_4/Co/CoO$ and $[Co/Pt]_5/IrMn$ multilayers [30–32]. However, all of the precedent MFM studies are based on the uniform magnetic field through the whole sample surface.

In this letter, we concentrate on the studies of the influence from the highly localized magnetic field of the MFM tip onto the perpendicular exchange bias Pt/Co/Pt/IrMn multilayers (with easy axis *out-of-plane*) as a function of tip-sample distance (d_{TS}) and tip magnetization direction. Magnetization reversal process in magnetic domains of submicron scale was directly observed and later on compared with our theoretical results. With a well-controlled tip-sample distance and the ex-situ tip magnetization reversal method (TMRM)[33], the local magnetization reversal of submicron domains in EB multilayers was achieved by the highly localized magnetic tip field (H_{tip}). Asymmetric magnetization reversal were triggered by local tip field with opposite directions. By utilizing the static magnetometer measurement and atomic scale micro-magnetic calculations, the asymmetric magnetization reversal process can be attributed to the pinned domain wall motion of FM layer coupled with irreversible rotation of AF spins. The results are helpful to explain the anomalous exchange bias training effect in Co/Pt/IrMn multilayers[34]. Potentially, it may also pave a way to map and manipulate the magnetic nano structures such as Skyrmions and vortices with high resolutions.

II. EXPERIMENT

A large specimen of Pt(3 nm)/Co(0.5 nm)/Pt(0.5 nm)/$Ir_{25}Mn_{75}$(IrMn)(4 nm) multilayers was deposited on a flat quartz substrate (5×2 cm^2) by magnetron sputtering at ambient temperature as shown in Fig. 1(a). The base pressure of the vacuum chamber was 2×10^{-5} Pa and the working Argon pressure was 0.40 Pa during deposition. The exchange bias was induced by a magnetic field of about 50 Oe, along the sample normal direction (denoted as -z direction), from a small magnet set on the back of the substrate. After deposition, the sample was cut into identical small pieces (5×5 mm^2) to investigate the static magnetic properties and MFM separately. One small piece was measured in VSM (vibrating sample magnetometer) of Mode 7407 with auto-rotation option by LakeShore Company (Fig. 3, dotted curve). The perpendicular exchange bias has been well established in the multilayers with H_E=160 Oe and H_C=470 Oe. Among various thickness of IrMn

layers, we chose 4 nm IrMn as the AF layer, so H_E is set to be smaller than H_C deliberately so that the magnetization of multilayers can stay stably in either up or down direction at zero field with respect to the magnetization history.

Another piece of the as-deposit sample was characterized by MFM (Nanoscan Ltd., Switzerland with magnetic tip from MicroMasch), operating at the constant height dynamical mode[33]. The tip is oscillating vertically (z-axis) with an amplitude of A_0 and scans along the fast axis (x axis) with a speed of 512 pixel/s, and forms the MFM image by also slowly scanning along the perpendicular direction (y axis). On top of each pixel, the tip will oscillate 166 cycles (the cantilever used there has a natural resonant frequency of 85 kHz). The sample magnetization reversal of a specific domain will happens first when the tip reaches the critical height of $d_{TS} = z_0 - A_0$ (the lowest turning point at an oscillating cycle of the MFM cantilever), where z_0 is the balanced tip-sample distance, as shown in Fig. 1(a). Because the tip oscillates much slower than the magnetization reversal process ($\lesssim$100 ps)[35], so the tip field can be considered as DC field source. In order to study the hysteresis behavior, the tip field needs to be varied, which was achieved by monitoring the frequency shift (Δf) versus distance (d_{TS}) curve above the *non-magnetic* regions where the magnetic field gradient is effectively zero. The method has been discussed in details in Ref. 33. For the ultrathin FM layer studied here, the central regions in large magnetic domains (usually over several square microns) can serve this role, as long as distance d_{TS} is much smaller than the domain size[36]. Here, the van der Waals force and the electrostatic force (with an uncompensated bias voltage of 0.56 V between the tip and sample) make up the total *non-magnetic* contribution[33,37]. The sensitivity of the tip-sample distance control method has been discussed elsewhere[33,37].

III. RESULTS AND DISCUSSION

The MFM tip used in this paper, is a Co(60 nm)/Cr(20 nm) coated NSC18-series MFM tip from Mikromasch Inc with a quasi-Octagonal-cone-shape confirmed by our scanning electron microscopy (SEM) studies. It has a full tip cone angle of 40 degree with a tip radius of 80 nm (measured in SEM). In order to quantitatively

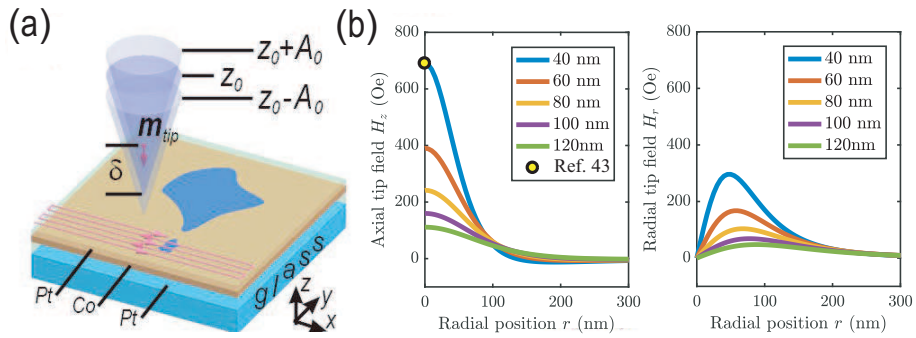

FIG. 1: (Color online) (a) Sketch of the local MFM probing method: an MFM tip carrying a moment of $M_{\rm tip}$ raster scan across the surface and the localized stray field induces magnetic reversal in Pt/Co/Pt/IrMn(hidden) multilayers. z_0 is the balanced tip-sample distance, A_0 is the oscillating amplitude and δ is the effective point-dipole position from the tip apex. (b)the vertical tip field (along z-axis) and the in plane radial tip field (along radial axis r) distributions versus radial position r at different d_{TS}. The solid circle dot is from Ref. 43.

study local hysteresis behaviour within one pixel sized square area (23.4×23.4 nm^2), the tip field was calculated using a magnetic point-dipole model [38,39] at various d_{TS} according to the following considerations: i) Great efforts have been put to quantitatively mapping the tip field using *e.g.*, Lorentz Microscopy (LM) within only a fixed plane (60±10 nm away from the tip apex) perpendicular to the tip axis [40,41]. For a similar pyramid-shaped CoCr coated tip with a similar tip height, the point-dipole model and the LM experiment have nearly shown the same radial distribution of the vertical H_z-field with same FWHMs. ii) in quantitative micromagnetic simulation [42], for a 50 nm thick Co coated tip, the effective dipole moment has been calculated to be $M_{\rm tip} = 3.14\times10^{-13}$ emu, which is also in agreement with the nominal value from the MFM tip supplier. iii) for the same MFM tip from the same supplier, another quantitative characterization has shown a tip field of 690 Oe at a d_{TS} of 40 nm [43], we have thus assumed the effective dipole position of $\delta \approx 55.4$ nm away from the tip apex (Fig.1(a)), which also shows good agreement with the micromagnetic simulation results (indicating effective dipole height in the range of 50∼100 nm) [42]. Based on above discussions,

the tip field H_z and H_r at different d_{TS} have been calculated based on a dipople moment of $M_{tip} = 3{\times}10^{-13}$ emu and an effective dipole height of $\delta = 55.4$ nm.

The in-plane radial MFM tip field H_r have been estimated in Fig. 1(b). Comparing H_r and H_z, one can easily see the tip field on top of each MFM image pixel is dramatically dominated by the axial field along z-direction. At smaller d_{TS}, H_r starts to play a role at about 2 pixel away (pixel size 23 nm here) and its maximal value is only less than half of the vertical field H_z. At larger d_{TS}, however, the peak in plane field component shifts away from the under scanned pixel location with larger H_z/H_r ratio. In summary, the in plane tip field has shown a smaller magnitude compared to the out-of-plane field, and additionally, its effect is also negligible compared to the out of plane H_C or H_E from our VSM results (Fig. S1), similar to other reported results [44]. Moreover, due to the high axial symmetric geometry of the MFM tip, we have considered the net in-plane field to be zero to the first order approximation.

With a highly localized MFM tip stray field[36,40], we can induce the nucleation of magnetization reversal processes in arbitrary regions, not necessary from the areas with lowest nucleation barriers, which happens in traditional magnetometry measurements as VSM[34] or Kerr microscopy[45] where a uniform field is normally applied to the whole sample. Figure 2 shows typical evolution of magnetic domains with various tip fields. In Fig. 2(a), the sample was set to the initial state with magnetization in $+z$ direction by external magnetic field of $\sim$1000 Oe. When lowering the MFM tip sample distance (d_{TS}), the tip field increased simultaneously in $-z$ direction. Thus small cores appeared in the $-z$ direction, called the nucleation process (Fig. 2(b)). With further increasing the tip field, domain wall (DW) motion took place and small cores merged into large magnetic domains as shown in Fig. 2(d). It is worth to mention that some already reversed domain such as the squared region in Fig. 2(b) can flip back to its previous magnetization direction under the same scanning condition as shown in Fig. 2(c). This indicates that there exists a small percent of coverage through the sample (not detectible by VSM), where the magnetization reversal process is possibly dominated by coherent rotation or creeping of DW [46], even there is no direct evidence from our VSM data. This shows the powerful local magnetic probing capability using MFM compared to

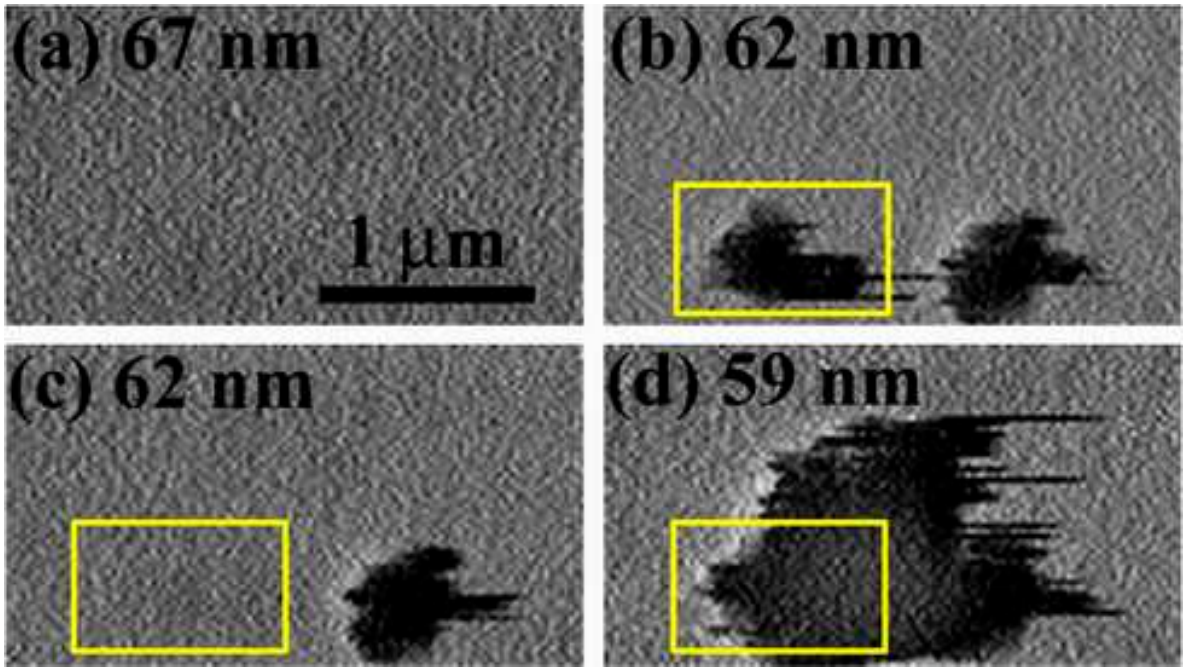

FIG. 2: (Color online) MFM images of the inhomogeneous domain nucleation and DW motion at different d_{TS} as indicated in panels (a)-(d). The uniform contrast in (a) indicates the magnetization in this whole scan area is along z, but the reversed ones in (b)-(d) are along $+z$ under -z tip fields. (b) and (c) are scanned under the same d_{TS} one after another with $d_{TS} = 62$ nm.

conventional magnetic metrologies. Unfortunately, due to the slow scanning speed of the MFM technique, the velocity dependent phenomenon, such as the creeping or the velocity of the pinned DW motion cannot be measured compared to the MOKE results [46].

The tip field cannot only induce the magnetization reversal in $-z$ direction, but also can induce the reversal in $+z$ direction with the help of TMRM. Figure 3 shows the evolution of a single domain under TMRM process. At d_{TS} of 107 nm, we start to see a reversed domain, with a size similar to the one shown in Fig. 2(c). Reduce further the tip height, one can see the growth of reversed domain and pinned DW motion directly in Fig.3(b). The growth of the domain is not isotropic, but biased towards the region on the lower side of the reversed domain (i.e., close to the regions marked by Squares 1 and 2). This indicates the distribution of DW propagation barriers is inhomogeneous[45]. Our result also confirms that the DW propagation

barrier is smaller than the nucleation barrier, in agreement with Ref. 10,45. The tip field with the same magnitude can induce more area of domains to reverse via DW propagation (the enlargement of existing domains) than DW nucleation (the creation of new domains). At smaller d_{TS}, i.e., shown in Fig. 2(c) and Fig. 3(b), we can also observe many spurious linear features along the fast-scan direction overlapped on the fractal domain profile. Whenever one lifts the tip to higher position, the spurious features will disappear, indicating reversible magnetization reversal processes. Hence, it is believed that the tip field can successfully assist either reversible or irreversible DW motion through the local pinning sites. In order to study the magnetization reversal behavior under an opposite tip field, TMRM has been applied. To do so, we have withdrawn the tip to a relative larger d_{TS} once we see very weak MFM contrast. By ex-situ TMRM[33], we have found the direct evidence for the asymmetry in the motion of the pinned DWs because the magnetization reversal is much easier than before at even higher d_{TS}. The d_{TS} are 196 ± 8 nm and 156 ± 6 nm in Figs. 3(c) and (d), respectively. The contrast of the reversed domain flips from *dark* to *bright*. Interestingly, the domain starts to shrink locally [*e.g.*, close to Square 2 in Fig. 3(c)] even when d_{TS} is still as large as 196 nm. Then at a distance d_{TS} of 156 nm [Fig. 3(d)], significant shrinking of the jagged domain is observed around the previously reversed domain. The large difference for the tip field dependent of pinned DW motion before and after TMRM is clearly related to the asymmetry of the FM magnetization reversal when the FM layer is exchange coupled by AF layer.

The local depinning fields can be reconstructed by the local effective hysteresis loops from a series of MFM images taken at different d_{TS} before and after TMRM and verified by the VSM results. With our method shown here, it is possible to study the exchange bias behavior in nanometer scale. We focus on the previously marked areas in Squares 1 and 2 (shown in Fig. 3), and the hysteresis loops are shown in Fig. 4, together with the VSM loop as a reference. For Squares 1 and 2, their local hysteresis loops show that the domain extension on the descending branch of the loop needs larger tip fields than the domain shrinking on the ascending branch to achieve magnetization reversal. By comparison of Square 1 and Square 2 of about 23.4×23.4 nm^2 in size, their H_C and H_E differs from each other, but both

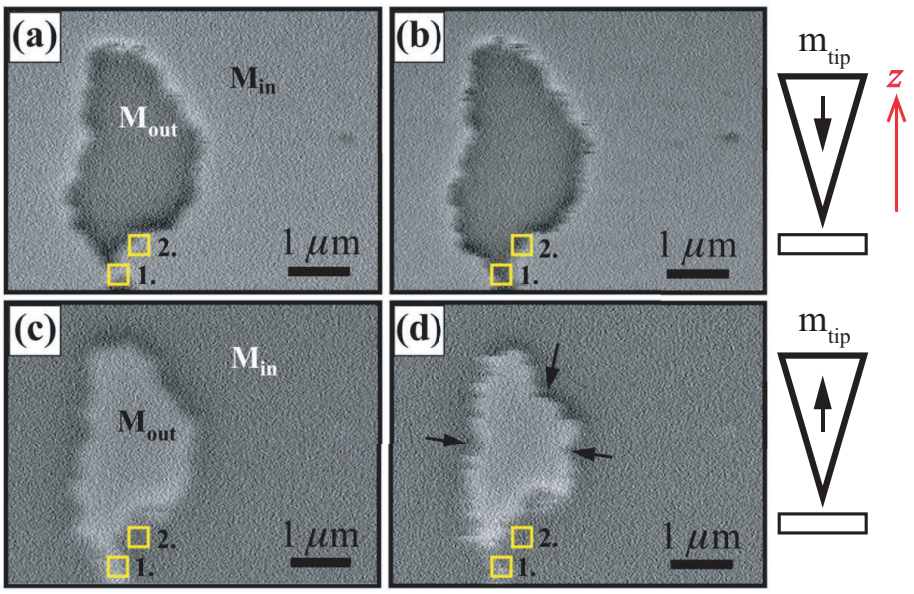

FIG. 3: (Color online) Selected MFM images of the evolution of FM domain structures at distances of (a) (107 ± 2) nm, (b) (79 ± 1) nm with -z tip fields, and (c) (196 ± 8) nm, (d) (156 ± 6) nm with $+z$ tip fields. Squares 1 and 2 are indicated in figures. Note that before and after TMRM, M_{in}/M_{out} has different contrast in upper panel ((a)-(b)) and lower panel ((c)-(d)), respectively.

much smaller than the value got from VSM, which is possible because only a 5 micron square area was reversed compared to the whole 12×12 microns^2 scan area, while the value from VSM reflects an average of the reversal process. Additionally, there are some area display much larger coercivity than the areas around Squares 1&2, indicated by black arrows in Fig. 3. With increased tip field, more nucleation sites can be observed (black arrows in Fig. 3(d)). The nucleation sites have a size around one hundred nanometer.

In order to have a better understanding of the local hysteresis behavior in perpendicular exchange biased sample, we have performed a theoretical calculation to study the pinning effect of the FM/AF system to quasi-quantitatively compare with our MFM results. This has been done by an atomistic model[47,48] using a classical Heisenberg spin Hamiltonian[49], where the spin dynamics is described by Landau-Lifshitz-Gilbert equation[50]. The thermal effect has also taken account into by using Langevin dynamics[51]. The perpendicular magnetocrystalline anisotropy of

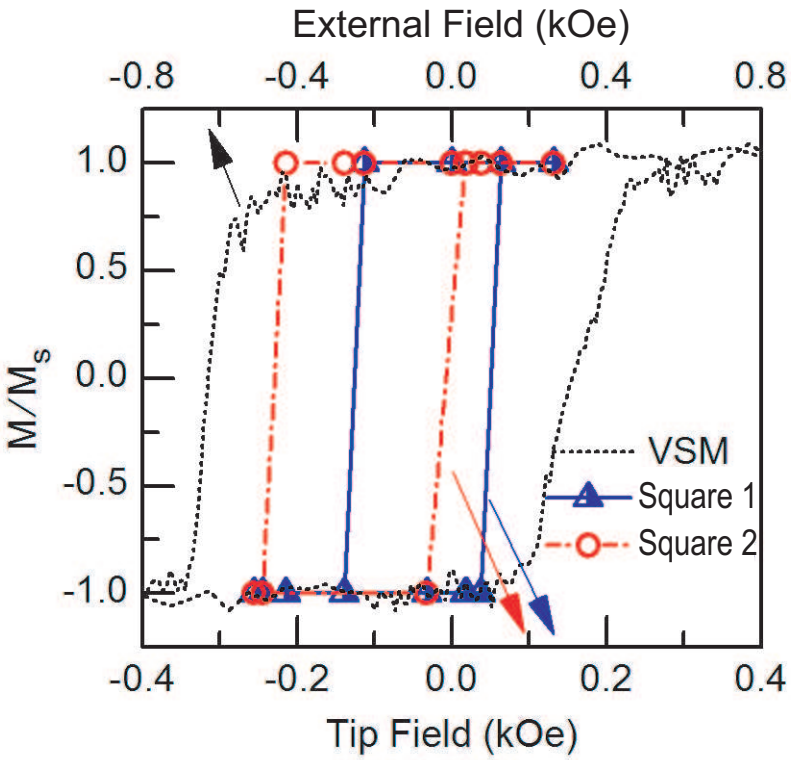

FIG. 4: (Color online) Two pixel sized hysteresis loops at Squares 1 and 2 shown in Fig. 3 as well as the VSM loop. The squared pixel size is 23.4×23.4 nm^2. Arrows indicate the reversed spotty contrast.

the FM layer is defined by a single ion uniaxial model. The AF layer is assumed to have an anisotropy far larger than the FM one, thus the AF is equal to an external field applied on the interface of the FM layer only, via the nearest neighboring exchange coupling. By varying the interfacial exchange coupling strength (J_{int}) and the anisotropy parameter of the FM layer, different hysteresis loops are obtained, corresponding to the magnetic properties of the different areas in the AF/FM sample. Figure 5 shows hysteresis loops with different interfacial exchange parameters (J_{int}) and pinning sites, simulating the magnetic characteristics of Squares 1&2 with difference of H_E and H_C. From the hysteresis loops, it can be seen the H_E and H_C are different from each other, and quasi-quantitatively comparable with the experimental results. This proves the depinning fields of the two local squares are different, and thus a domain will nucleate at the square with lower depinning field and then propagate to the area with higher depinning

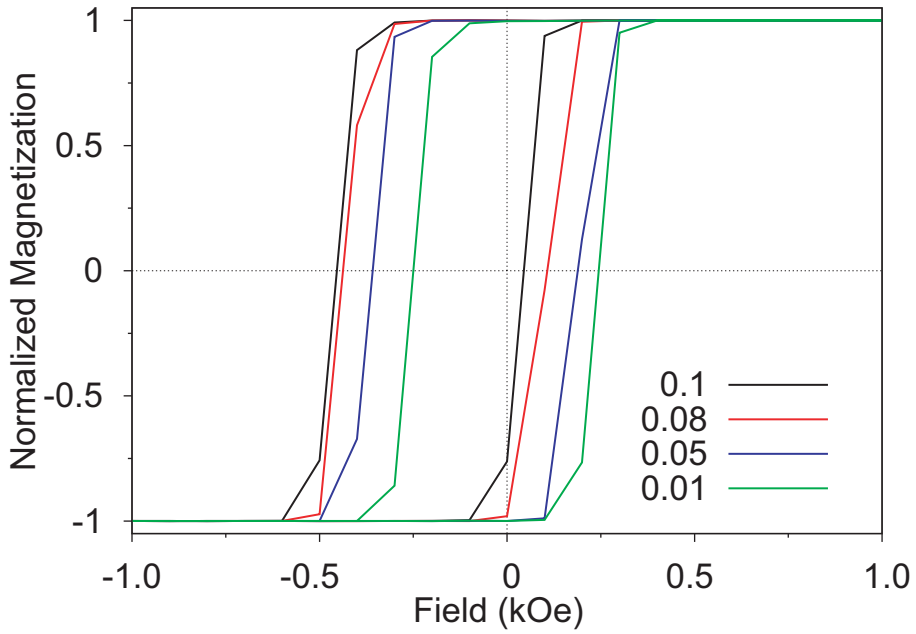

FIG. 5: (Color online) Calculated local hysteresis loops using atomistic model with different AF-FM interfacial exchange strength J_{int} ($\times 10^{-21}$ J).

field. Moreover, it should be noted, the evolution of magnetic domains in upward and downward directions may also be affected by the different configurations of AF spins in Pt/Co/Pt/IrMn multilayers[52]. Hereby, our theoretical simulation has shown very good agreement with our experimental MFM results.

IV. CONCLUSION

In summary, the asymmetric magnetization reversal in exchange biased Pt/Co/Pt/IrMn multilayers is studied by using local fields of the MFM tips and shown to be accomplished by inhomogeneous domain nucleation followed by the pinned DW motion which is asymmetric under opposite tip fields. We demonstrated an ability to determine local variation in critical fields for domain nucleation as well as pinned DW motions with nanoscale resolution. This opens the door for a more systematic study of the effect of disorder and their spatial distribution on our understanding of the EB effect in nanostructure materials. The results may shed

new light on the detection and manipulation of magnetic nano structures such as Skyrmions and vortices.

Acknowledgments

The authors acknowledge A. Asenjo for fruitful discussions about the MFM tip field analysis and S. McVitie for helpful inputs in the quantitative characterization of the MFM tip field using Lorentz microscopy. National High Technology Research and Development Program of China (Grant2002AA302103), the National Natural Science Foundation of China under Grant No. 11774259, 51501131 are greatly acknowledged.

[1] W. H. Meiklejohn and C. P. Bean, Phys. Rev. **102**, 1413 (1956).

[2] E. Berkowitz and K. Takano, J. Magn. Magn. Mater. **200**, 552 (1999).

[3] J. Nogués and I. K. Schuller, J. Magn. Magn. Mater. **192**, 203 (1999).

[4] H. Ohldag, A. Scholl, F. Nolting, E. Arenholz, S. Maat, A. T. Young, M. Carey, and J. Stöhr, Phys. Rev. Lett. **91**, 017203 (2003).

[5] K. Takano, R. H. Kodama, A. E. Berkowitz, W. Cao, and G. Thomas, Phys. Rev. Lett. **79**, 1130 (1997).

[6] I. Schmid, P. Kappenberger, O. Hellwig, M. J. Carey, E. E. Fullerton, and H. J. Hug, Europhys. Lett. **81**, 17001 (2008).

[7] C. Chappert, A. Fert, and F. N. Van Dau, Nat Mater **6**, 813 (2007).

[8] W. O. Rosa, L. Martínez, M. Jaafar, A. Asenjo, and M. Vázquez, J. Appl. Phys. **106**, 103906 (2009).

[9] M. T. Rahman, N. N. Shams, D. S. Wang, and C.-H. Lai, Appl. Phys. Lett. **94**, 082503 (2009).

[10] S. Laureti, S. Y. Suck, H. Haas, E. Prestat, O. Bourgeois, and D. Givord, Phys. Rev. Lett. **108**, 077205 (2012).

[11] F. Fettar, L. Cagnon, and N. Rougemaille, Appl. Phys. Lett. **97**, 192502 (2010).

[12] S. Giri, M. Patra, and S. Majumdar, J. Phys.: Condens. Matter **23**, 073201 (2011).

[13] J. Nogués, J. Sort, V. Langlais, V. Skumryev, S. Surinach, J. Munoz, and M. Baró, Phys. Rep. **422**, 65, (2005).

[14] D. Tripathy and A. O. Adeyeye, Phys. Rev. B **79**, 064413 (2009).

[15] X. Gao, X. P. Qiu, Z. Shi, S. M. Zhou, X. J. Bai, and J. Du, J. Phys. D: Appl. Phys. **42**, 065003 (2009).

[16] X. F. Han, Z. C. Wen, and H. X. Wei, J. Appl. Phys. **103**, 07E933 (2008).

[17] G. Yu, A. Jenkins, X. Ma, S. A. Razavi, C. He, G. Yin, Q. Shao, Q. lin He, H. Wu, W. Li, W. Jiang, X. Han, X. Li, A. C. Bleszynski Jayich, P. K. Amiri, and K. L. Wang, Nano Lett. 18, 980 (2018).

[18] X. Ma, G. Yu, S. A. Razavi, S. S. Sasaki, X. Li, K. Hao, S. H. Tolbert, K. L. Wang, and X. Li, Phys. Rev. Lett. 119, 027202 (2017).

[19] W. Jiang, P. Upadhyaya, W. Zhang, G. Yu, M. B. Jungfleisch, F. Y. Fradin, J. E. Pearson, Y. Tserkovnyak, K. L. Wang, O. Heinonen, S. G. E. te Velthuis, and A. Hoffmann, Science **349**, 283 (2015).

[20] W. Legrand, D. Maccariello, N. Reyren, K. Garcia, C. Moutafis, C. Moreau-Luchaire, S. Collin, K. Bouzehouane, V. Cros, and A. Fert, Nano Lett. **17**, 2703 (2017).

[21] Y. Li, N. Kanazawa, X. Z. Yu, A. Tsukazaki, M. Kawasaki, M. Ichikawa, X. F. Jin, F. Kagawa, and Y. Tokura, Phys. Rev. Lett. **110**, 117202 (2013).

[22] G. Chen, A. Mascaraque, A. T. NDiaye, and A. K. Schmid, Appl. Phys. Lett. **106**, 242404 (2015).

[23] O. Boulle, J. Vogel, H. Yang, S. Pizzini, D. de S. Chaves, A. Locatelli, T. O. Mente, A. Sala, L. D. Buda-Prejbeanu, O. Klein, M. Belmeguenai, Y. Roussign, A. Stashkevich, S. M. Chérif, L. Aballe, M. Foerster, M. Chshiev, S. Auffret, I. M. Miron, and G. Gaudin, Nat. Nanotech. **11**, 449 (2016).

[24] B. F. Miao, L. Sun, Y. W. Wu, X. D. Tao, X. Xiong, Y. Wen, R. X. Cao, P. Wang, D. Wu, Q. F. Zhan, B. You, J. Du, R. W. Li, and H. F. Ding, Phys. Rev. B **90**, 174411 (2014).

[25] A. Soumyanarayanan, M. Raju, A. L. G. Oyarce, A. K. C. Tan, M.-Y. Im, A. P. Petrovi, P. Ho, K. H. Khoo, M. Tran, C. K. Gan, F. Ernult, and C. Panagopoulos, Nat. Mater. **16**, 898 (2017).

[26] P. Milde, D. Khler, J. Seidel, L. M. Eng, A. Bauer, A. Chacon, J. Kindervater, S. Mhlbauer, C. Pfleiderer, S. Buhrandt, C. Schtte, and A. Rosch, Science **340**, 1076 (2013).

[27] J.-G. Zhu, Y. Zheng, and X. Lin, J. Appl. Phys. **81**, 4336 (1997).

[28] A. Mougin, S. Poppe, J. Fassbender, B. Hillebrands, G. Faini, U. Ebels, M. Jung, D. Engel, A. Ehresmann, and H. Schmoranzer, J. Appl. Phys. **89**, 6606 (2001).

[29] J. Sort, A. Hoffmann, S.-H. Chung, K. S. Buchanan, M. Grimsditch, M. D. Baró, B. Dieny, and J. Nogués, Phys. Rev. Lett. **95**, 067201 (2005).

[30] P. Kappenberger, S. Martin, Y. Pellmont, H. J. Hug, J. B. Kortright, O. Hellwig, and E. E. Fullerton, Phys. Rev. Lett. **91**, 267202 (2003).

[31] X. Ji, A. B. Pakhomov, and K. M. Krishnan, J. Appl. Phys. **101**, 09E507 (2007).

[32] I. Schmid, M. A. Marioni, P. Kappenberger, S. Romer, M. Parlinska-Wojtan, H. J. Hug,

O. Hellwig, M. J. Carey, and E. E. Fullerton, Phys. Rev. Lett. **105**, 197201 (2010).

[33] H. Zhong, W. Peng, G. Tarrach, A. Drechsler, J. Jiang, D. Wei, and J. Yuan, J. Phys. D: Appl. Phys. **41**, 085002 (2008).

[34] Z. Shi, X. P. Qiu, S. M. Zhou, X. J. Bai, and J. Du, Appl. Phys. Lett. **93**, 222504 (2008).

[35] S. Mizukami, E. P. Sajitha, D. Watanabe, F. Wu, T. Miyazaki, H. Naganuma, M. Oogane, and Y. Ando, Appl. Phys. Lett. **96**, 152502 (2010).

[36] P. J. A. van Schendel, H. J. Hug, B. Stiefel, S. Martin, and H.-J. Güntherodt, J. Appl. Phys. **88**, 435 (2000).

[37] H. Zhong, L. Huang, D. Wei, S. Wang, Y. Zhu, and J. Yuan, J. Magn. Magn. Mater. **321**, L37 (2009). .

[38] J. D. Jackson, "Classical Electrodynamics" (3rd ed.). New York: Wiley. ISBN 978-0-471-30932-1. (1998).

[39] J. Lohau, S. Kirsch, A. Carl, G. Dumpich, and E. F. Wassermann, J. Appl. Phys. **86**, 3410 (1999).

[40] S. McVitie, R. P. Ferrier, J. Scott, G. S. White, and A. Gallagher, J. Appl. Phys. **89**, 3656 (2001).

[41] J. Scott, S. McVitie, R. P. Ferrier, and A. Gallagher, J. Phys. D: Appl. Phys. **34**, 1326 (2001).

[42] H. Li, Y. Wang, S. Wang, H. Zhong, and D. Wei, IEEE Trans. Magn. **46**, 2570 (2010).

[43] M. Jaafar, A. Asenjo, and M. Vzquez, IEEE Trans. Nanotech. **7**, 245 (2008).

[44] Y. Nie, W. W. Lin, M. Huang, K. X. Xie, J. Du, H. Sang, and G. Xiao, J. Appl. Phys. **103**, 07C110 (2008).

[45] F. Romanens, S. Pizzini, F. Yokaichiya, M. Bonfim, Y. Pennec, J. Camarero, J. Vogel, J. Sort, F. Garcia, B. Rodmacq, and B. Dieny, Phys. Rev. B **72**, 134410 (2005).

[46] P. J. Metaxas, J. P. Jamet, A. Mougin, M. Cormier, J. Ferré, V. Baltz, B. Rodmacq, B. Dieny, and R. L. Stamps, Phys. Rev. Lett. 99, 217208 (2007).

[47] R. F. L. Evans, W. J. Fan, P. Chureemart, T. A. Ostler2, M. O. A. Ellis and R. W. Chantrell, J. Phys.: Condens. Matter. **26**, 103202 (2014).

[48] W. J. Fan, E. F. L. Evans, Y. Hancock, and R. W. Chantrell, J. Appl. Phys. **109**, 07B752 (2011).

[49] W. Heisenberg, Zeitschrift fur Physik, **49**, 619 (1928).

[50] T.L. Gilbert. Phys. Rev., **100**, 1243 (1955).

[51] W. F. Brown, Jr., IEEE Trans. Magn. **15**, 1196 (1979).

[52] Y. Y. Wang, C. Song, B. Cui, G. Y. Wang, F. Zeng, and F. Pan, Phys. Rev. Lett. **109**, 137201 (2012).